Research article

PPARα inhibits vascular smooth muscle cell proliferation underlying intimal hyperplasia by inducing the tumor suppressor p16INK4a

Florence Gizard,[1] Carole Amant,[2] Olivier Barbier,[1] Stefano Bellosta,[3] Romain Robillard,[1] Frédéric Percevault,[1] Henry Sevestre,[2] Paul Krimpenfort,[4] Alberto Corsini,[3] Jacques Rochette,[2] Corine Glineur,[1] Jean-Charles Fruchart,[1] Gérard Torpier,[1] and Bart Staels[1]

[1]INSERM U545, Département d'Athérosclérose, Institut Pasteur de Lille et Faculté de Pharmacie, Université Lille II, Lille, France.
[2]CHU d'Amiens et Faculté de Médecine, Université Jules Verne de Picardie, Amiens, France. [3]Department of Pharmacological Sciences, University of Milan, Milan, Italy. [4]Division of Molecular Genetics and Centre for Biomedical Genetics, The Netherlands Cancer Institute, Amsterdam, The Netherlands.

Vascular SMC proliferation is a crucial event in occlusive cardiovascular diseases. PPARα is a nuclear receptor controlling lipid metabolism and inflammation, but its role in the regulation of SMC growth remains to be established. Here, we show that PPARα controls SMC cell-cycle progression at the G_1/S transition by targeting the cyclin-dependent kinase inhibitor and tumor suppressor p16INK4a (p16), resulting in an inhibition of retinoblastoma protein phosphorylation. PPARα activates *p16* gene transcription by both binding to a canonical PPAR-response element and interacting with the transcription factor Sp1 at specific proximal Sp1-binding sites of the p16 promoter. In a carotid arterial–injury mouse model, p16 deficiency results in an enhanced SMC proliferation underlying intimal hyperplasia. Moreover, PPARα activation inhibits SMC growth in vivo, and this effect requires p16 expression. These results identify an unexpected role for p16 in SMC cell-cycle control and demonstrate that PPARα inhibits SMC proliferation through p16. Thus, the PPARα/p16 pathway may be a potential pharmacological target for the prevention of cardiovascular occlusive complications of atherosclerosis.

Introduction

Activation of vascular SMC proliferation is a key event in the development of atherosclerosis and its complications (1). In response to vascular injury, SMCs migrate from the media into the intimal layer of the arterial wall, where they proliferate and synthesize extracellular matrix, resulting in the formation of intimal hyperplasia. In this process, vascular SMCs undergo phenotypic changes from a differentiated and contractile state to a dedifferentiated and synthetic state (2). (Dys)regulation of SMC growth occurs thus during atherosclerotic plaque formation as part of a local inflammatory response in association with accumulation of lipids and fibrous connective tissue in the vascular wall (3). SMC proliferation is also the primary pathophysiological mechanism underlying complications of procedures used to treat atherosclerotic diseases, such as restenosis, a secondary occlusion of the arterial wall following transluminal angioplasty or stent implantation, and vein bypass graft failure (1).

As a key early event in these phenotypic changes, SMCs, which are in a quiescent state (G_0) in normal uninjured vessels, transit through the G_1 phase of the cell cycle and enter into the S phase to undergo replication (4). Cell-cycle progression is under the control of cyclin-dependent kinases (CDKs), which phosphorylate different specific target proteins through the 4 stages of the cell cycle (5). Notably, phosphorylation of the retinoblastoma gene product (pRB) by the specific G_1 CDKs represents the critical checkpoint of G_1/S transition (6). When underphosphorylated, pRB sequesters the E2F family transcription factors, which regulate genes encoding proteins required for S phase DNA synthesis. Phosphorylation of pRB releases E2F that permits the induction of E2F-dependent genes and therefore the irreversible induction of the mitosis process, after which cells are refractory to extracellular growth-inhibition signals. Thus, increased pRB phosphorylation correlates with the induction of SMC proliferation in injured vessels (1, 6). As CDKs are constitutively present in each phase of the cell cycle, CDK-mediated pRB phosphorylation is respectively activated or inhibited through timely interactions with expressed cyclins and CDK inhibitors (CDKIs) (7). Notably, the CDKI p16 is a tumor suppressor transcriptionally regulated by pRB, which plays a key role in the control of pRB phosphorylation and G_1/S cell-cycle progression (8–11).

PPARα is a nuclear receptor that, upon ligand activation, regulates transcription after dimerizing with the retinoid X receptor (RXR) and DNA-binding to PPAR-response elements (PPREs) within the regulatory regions of target genes (12). PPREs usually consist of a direct repeat of the hexanucleotide AGGTCA sequence separated by 1 or 2 nucleotides (DR1 or DR2) (12). Furthermore, PPARα can also negatively interfere with proinflammatory signaling pathways by a mechanism termed "transrepression" (13). PPARα is activated by natural ligands such as fatty acids and derivatives (13). Notably, natural eicosanoids derived from arachidonic acid via the lipoxygenase pathway as well as oxidized phospholipids activate PPARα (13). Moreover, fibrates (gemfibrozil, bezafibrate, ciprofibrate, and fenofibrate), synthetic drugs initially used to treat lipid disorders (14), act as PPARα ligands (15).

Figure 1

PPARα inhibits SMC G$_1$/S progression. (**A** and **B**) G$_1$-arrested hSMCs (**A**) and PPARα$^{-/-}$ or PPARα$^{+/+}$ Sv/129 mSMCs (**B**) resumed growth at T0 in normal GM. The indicated concentrations of GW7647, Wy14,643 (10 μM), or vehicle (Me$_2$SO) were added in the normal GM. Cells were harvested at the indicated times for measure of DNA content (expressed as arbitrary units). Values are the mean ± SEM of triplicate points from a single experiment (n = 3/time point), which was repeated with 3 different cell preparations of primary SMCs with similar results. *P ≤ 0.05; ***P ≤ 0.001 vs. vehicle-treated hSMCs (**A**). Values in **B** followed by different symbols are statistically significantly different from each other. (**C**) Western blot analysis of in-cell pRB phosphorylation was performed using an anti-pRB antibody recognizing all species of the Rb gene product on protein extracts (30 μg) from Ad-GFP or Ad-PPARα–infected hSMCs and treated with vehicle or GW7647 (600 nM) for 10 hours.

Fibrates have been shown to decrease morbidity and mortality of cardiovascular diseases (16) and impede the progression of coronary atherosclerotic lesions when administered to postinfarction or diabetic patients (17–19). PPARα mediates their systemic metabolic effects by regulating genes encoding proteins involved in lipid and lipoprotein metabolism (20). Recently, the functions of PPARα have been extended to a regulatory action on cholesterol homeostasis and vascular inflammation acting directly at the level of the vascular wall, which could confer additional protective effects in the prevention of atherogenesis (13). Importantly, PPARα is also highly expressed in SMCs isolated from vascular tissues and from atherosclerotic lesions (21–23), where it controls IL-1–induced secretion of IL-6 and production of prostaglandins by inhibiting *IL-6* and *COX2* gene transcription. However, although recent studies have indicated that fibrates may regulate SMC proliferation in vitro (21, 24), a role for PPARα in SMC cell-cycle control has not yet been explored. In the present study, we demonstrate a role for PPARα in the control of SMC G$_1$/S transition. Moreover, we identify the CDKI p16 as an important controller of vascular SMC proliferation and show that p16 mediates the effects of PPARα on SMC proliferation both in vitro and in vivo.

Results

PPARα inhibits SMC proliferation by controlling cell-cycle progression into the S phase. Previous studies have indicated that certain fibrates may regulate human SMC (hSMC) proliferation in vitro (21, 24). To further analyze the effect of PPARα activation on SMC growth, the influence of a novel generation subtype-specific PPARα agonist, GW7647, which presents a high affinity (EC50 = 6 nM) and specificity (~200-fold selectivity over PPARγ and PPARδ) (25), was first tested on hSMCs resuming proliferation in normal growth medium (GM) after G$_0$/G$_1$-phase synchronization (Figure 1A). Whereas vehicle-treated cells displayed a growth rate comparable to that of untreated cells (not shown) with a doubling time of approximately 24 hours, GW7647 treatment inhibited proliferation in a dose-dependent manner. To examine which stage(s) of the cell-cycle is (are) regulated by GW7647, the cell-cycle distribution of hSMCs resuming growth in GM was analyzed by flow cytometry analysis after 48 hours of treatment with GW7647 or vehicle. As shown in Table

1, GW7647 treatment increased and decreased the proportion of hSMCs in the G$_0$/G$_1$ and S phases, respectively.

To further characterize the exact role of PPARα in SMC cell-cycle control, aortic mouse SMCs (mSMCs) were isolated from PPARα$^{-/-}$ and PPARα$^{+/+}$ mice. Interestingly, PPARα$^{-/-}$ mSMCs isolated from both Sv/129 (Figure 1B) and C57BL/6J (Supplemental Figure 1; supplemental material available online with this article; doi:10.1172/JCI22756DS1) genetic backgrounds proliferated at a much higher rate than corresponding PPARα$^{+/+}$ mSMCs. Moreover, incubation of mSMCs with Wy14,643, a specific murine PPARα agonist, inhibited cell proliferation of PPARα$^{+/+}$, but not PPARα$^{-/-}$ mSMCs (Figure 1B). Similarly to hSMCs, PPARα activation of mSMCs (assessed after 48-hour treatment in GM) was associated with a higher cell percentage in G$_0$/G$_1$ and a concomitant decrease of cell percentage in the S phase (Table 1).

Concomitantly, phosphorylation of pRB, the major checkpoint of G$_1$/S progression (5), was reduced in GW7647-treated hSMCs, an effect which was even more pronounced upon infec-

Table 1

PPARα negatively controls SMC G$_1$/S cell-cycle progression

	Cell cycle distribution (%)		
	G$_0$/G$_1$	S	G$_2$/M
hSMCs			
Vehicle (Me$_2$SO)	31.1 ± 4.2	57.1 ± 4.0	12.8 ± 4.5
GW7647	63.7 ± 5.6[A]	20.1 ± 2.6[A]	16.2 ± 4.8[B]
mSMCs			
PPARα$^{+/+}$, vehicle	65.2 ± 3.4	20.2 ± 1.9	14.6 ± 1.1
PPARα$^{+/+}$, Wy14,643	74.2 ± 7.2[C]	11.7 ± 7.2[C]	14.1 ± 1.2[D]
PPARα$^{-/-}$, vehicle	39.5 ± 5.1[E]	48.7 ± 6.2[E]	11.8 ± 2.5[D]
PPARα$^{-/-}$, Wy14,643	35.2 ± 6.3[E]	50.0 ± 3.2[E]	14.8 ± 3.1[D]

G$_1$-synchronized SMCs were induced to proliferate by reincubation in normal GM. GW7647 or Wy14,643 (50 μM) was added simultaneously in GM of hSMCs and Sv/129 mSMCs, respectively. After 48 hours, cells were harvested for flow cytometry profile analyses. Values are mean ± SEM of values obtained from 2 independent experiments performed in triplicate (n = 6/time point). [A,C,E]P ≤ 0.001 vs. vehicle-treated hSMCs. [B,D]NS. For mSMCs, values followed by different footnote letters are statistically significantly different from each other.
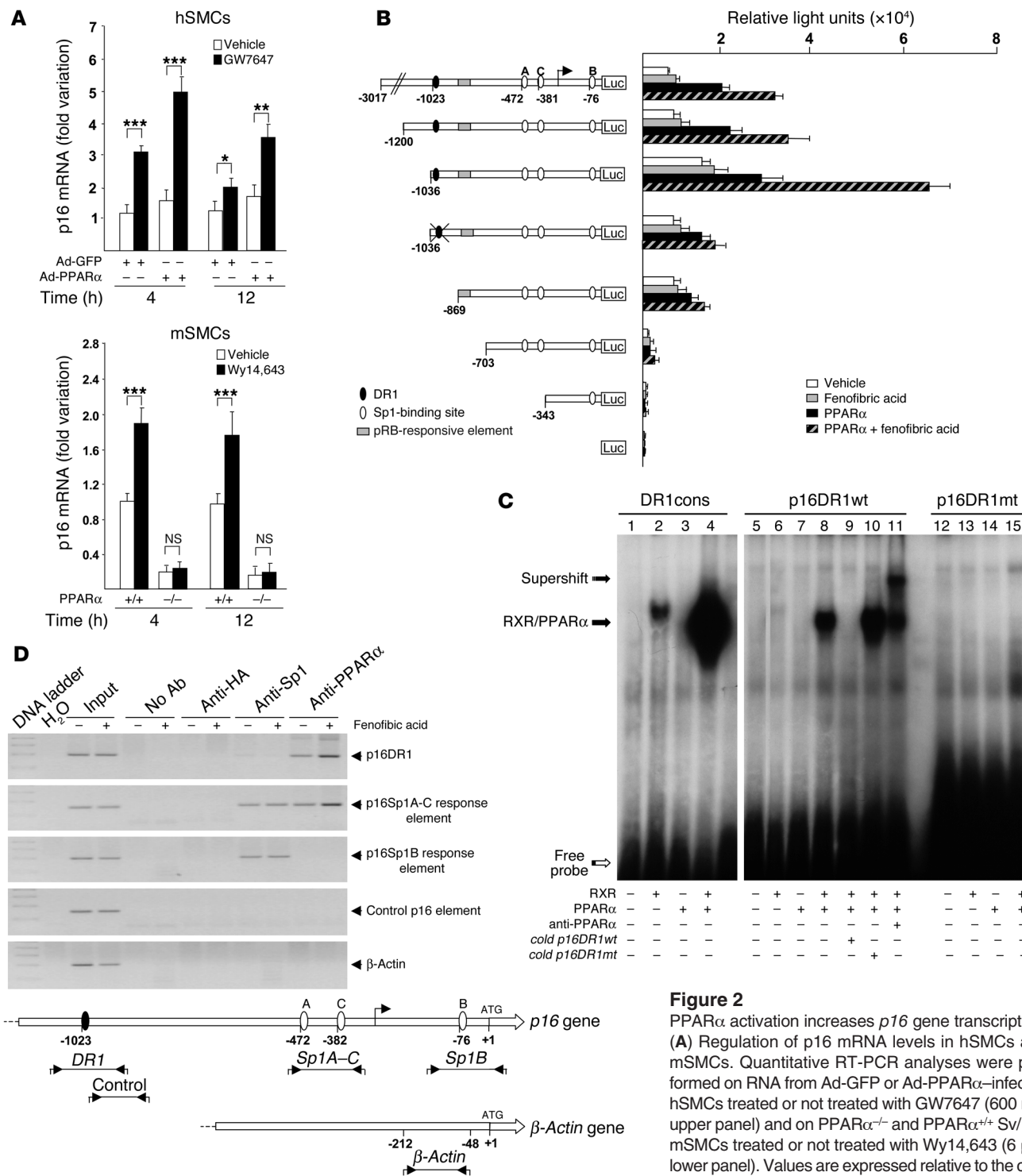
Figure 2

PPARα activation increases *p16* gene transcription. (**A**) Regulation of p16 mRNA levels in hSMCs and mSMCs. Quantitative RT-PCR analyses were performed on RNA from Ad-GFP or Ad-PPARα–infected hSMCs treated or not treated with GW7647 (600 nM, upper panel) and on PPARα−/− and PPARα+/+ Sv/129 mSMCs treated or not treated with Wy14,643 (6 μM, lower panel). Values are expressed relative to the controls (mRNA levels in PPARα+/+ mSMCs or hSMCs at T0) set as 1. (**B**) Induction of human *p16* promoter activity by ligand-activated PPARα. pGL2 luciferase reporter constructs driven by the indicated *p16* promoter deletion fragments (0.1 μg) were cotransfected in HeLa cells with or without pSG5 PPARα expression plasmid (0.3 μg). Cells were subsequently treated with fenofibric acid (100 μM) for 10 hours. Results (mean ± SD) from 1 representative experiment (*n* = 3) out of 3 is shown. (**C**) In vitro binding of PPARα to the p16DR1. EMSAs were carried out with end-labeled consensus DR1 (DR1cons), wild-type p16DR1 (p16DR1wt), or mutated p16DR1 (p16DR1mt) probes in the presence of unprogrammed reticulocyte lysate, RXR, PPARα, or both RXR and PPARα as indicated. (**D**) In-cell occupation of the *p16* gene promoter by PPARα. Soluble chromatin was prepared from hSMCs treated with or without fenofibric acid (250 μM). IP was performed with anti-Sp1 or anti-PPARα antibodies, and DNA was amplified using specific primer pairs. Bottom lane shows schematic diagram depicting the fragments of the *p16* and β-*actin* genes that were amplified. The nucleotide positions are indicated relative to the ATG. In panels **B** and **D**, A, B, and C denote the 3 Sp1-binding sites identified by Myohanen et al. (26) (see Results), and the putative transcription start site of the *p16* promoter is indicated by an arrow.

Table 2
Oligonucleotides used in this study

Name	Use	Orientation	Sequence	Refs.
hp16	PCR	s	5′-ATGCACGTGAAGCCATTGCGA-3′	
		as	5′-AAGTTTCCCGAGGTTTCTCAGAGCC-3′	
mp16	PCR	s	5′-CGTACCCCGATTCAGGTGAT-3′	
		as	5′-TTGAGCAGAAGAGCTGCTACGT -3′	
28S	PCR	s	5′-AAACTCTGGTGGAGGTCCGT-3′	(64)
		as	5′-CTTACCAAAAGTGGCCCACTA-3′	
β-actin	PCR	s	5′-GATGACCCAGATCATGTTTGA-3′	(64)
		as	5′-CGGATGTCAACGTCACACTTCATG-3′	
p16DR1	ChIP	s	5′-GCACTCATATTCCCTTCCCCCCT-3′	
		as	5′-GGAAGGACGGACTCCATTCTCAAAG-3′	
p16Sp1A–C	ChIP	s	5′-CCCCGATTCAATTTGGCAGTTAGG-3′	
		as	5′-CAGCGTTGGCAAGGAAGGAGGA-3′	
p16Sp1B	ChIP	s	5′-CCAGAGGATTTGAGGGACAGGGTC-3′	
		as	5′-AGTCAGCCGAAGGCTCCATGCT-3′	
p16 control	ChIP	s	5′-GAAGCTGGTCTTTGGATCACTGTGC-3′	
		as	5′-GACGGGGGAGAATTCTGCCTGT-3′	
β-actin	ChIP	s	5′-AAACTCTCCCTCCTCCTCTTCCT-3′	(54)
		as	5′-CGAGCCATAAAAGGCAACTTTCG-3′	
DR1cons	Gel shift	s	5′-AGGTCA A AGGTCA-3′	
p16DR1wt	Gel shift transfection	s	5′-GTGTGAA<u>AGGAGAC</u>AGGAC<u>A</u>GTATTT-3′	
p16DR1mt	Gel shift	s	5′-GTGTGAA**CC**AGAC<u>A</u>GGAC<u>A</u>GTATTT-3′	
Sp1A	Gel shift	s	5′-AAGGAAAC<u>GGGGCGGGGG</u>CGGATTTCTTT-3′	(26)
Sp1B	Gel shift	s	5′-CAGAGGGT<u>GGGGCGGA</u>CCGCGTGCGCTCG-3′	
Sp1C	Gel shift	s	5′-CAGGGAGGCCGG<u>AGGGCGGT</u>GTGGGGGGCA-3′	

Underlined nucleotides represent PPARα response element half-sites. Nucleotides in bold are mutated. p16Sp1A is the Sp1-binding site of the proximal promoter of p16 denoted A by Myohanen et al. (26). DR1cons, consensus DR1; s, sense; as, antisense.

tion with adenovirus-PPARα (Ad-PPARα) (Figure 1C). Altogether, these results indicate that PPARα activation inhibits both human and mouse vascular SMC proliferation by interfering with G$_1$/S cell-cycle progression.

PPARα induces transcription of the G$_1$/S transition regulator and tumor suppressor p16. Since PPARα is a nuclear receptor acting at the transcriptional level (12) and since the tumor suppressor p16 is a transcriptionally regulated CDKI controlling G$_1$/S cell-cycle progression functionally related to in-cell pRB expression and phosphorylation levels (8–10), we hypothesised that p16 could be a PPARα target gene. Indeed, in both mSMCs and hSMCs, p16 mRNA levels were increased upon PPARα agonist incubation (Figure 2A). The induction of p16 mRNA occurred in a PPARα-dependent manner and was already evident within 4 hours of treatment (Figure 2A). In hSMCs, the increase of p16 mRNA levels upon GW7647 treatment was more pronounced in Ad-PPARα–infected hSMCs (Figure 2A, upper panel). Moreover, Wy14,643 treatment induced p16 expression in PPARα$^{+/+}$, but not in PPARα$^{-/-}$ mSMCs (Figure 2A, lower panel). Interestingly, p16 mRNA levels were decreased by approximately two-thirds in PPARα$^{-/-}$ compared with PPARα$^{+/+}$ mSMCs.

Previously, a pRB-responsive site and proximal Sp1-binding sites (denoted A, B, and C) have been shown to be involved in the basal activity of the *p16* promoter (11, 26). Here, the presence of a putative degenerated DR1 PPRE sequence (AGGAGACAGGACA) at position –1023 to –1011 (denoted the p16DR1 site) was also revealed by computer-assisted analysis. To investigate the putative function of these elements in mediating the response to lig-

and-activated PPARα, reporter constructs driven by different *p16* promoter fragments were cotransfected with or without the pSG5-PPARα expression plasmid, and cells were subsequently treated with the PPARα agonists fenofibric acid or GW7647. Cotransfection of PPARα followed by ligand activation significantly induced activity of the –3.0-kb *p16* gene promoter, indicating that *p16* is a direct PPARα target gene (Figure 2B). PPARα-dependent *p16* promoter activation was maintained upon 5′ deletion to –1.0 kb. Further nucleotide deletions to –869 and –703 bp, as well as mutation of p16DR1, resulted in a significant, albeit incomplete reduction of *p16* promoter activation by PPARα. Finally, deletion to –343 bp completely abolished activation of the *p16* promoter by fenofibric acid–activated PPARα (Figure 2B). Identical results were obtained in cells treated with GW7647 (250 nM) (data not shown). These observations indicate that both p16DR1 and Sp1A–C elements are involved in PPARα-dependent *p16* promoter activation, with the DR1 element mediating the majority of the response.

To determine whether PPARα physically binds to the p16DR1 site, electrophoretic mobility shift assays (EMSAs) were performed using in vitro–produced PPARα and RXR proteins and double-stranded [^{32}P]-labeled oligonucleotides (Table 2 and Figure 2C). Whereas neither RXR nor PPARα alone bound to the p16DR1 probe, a clear shift was observed upon incubation with both RXR and PPARα. This complex was supershifted by the anti-PPARα antibody and prevented by an excess of unlabeled wild-type, but not mutated, p16DR1 probe. Moreover, the mutated p16DR1 probe did not bind RXR/PPARα (Figure 2C). These results demonstrate that the RXR/PPARα heterodimer specifically binds in vitro to the p16DR1 site located at –1023 pb. In contrast, no PPARα/DNA complex formation was detected in EMSAs performed with oligonucleotides overlapping the proximal Sp1A- and B-binding sites (data not shown).

To investigate the in vivo occupancy of these p16DR1 and Sp1-binding sites by activated PPARα, chromatin IP (ChIP) assays were performed on DNA from hSMCs treated or not treated with fenofibric acid using anti-Sp1 and anti-PPARα antibodies (Figure 2D). In accordance with the EMSA results, the region spanning the p16DR1 sequence was immunoprecipitated by the anti-PPARα antibody, an effect which was enhanced by fenofibric acid treatment. In addition, in agreement with results of Myöhänen et al. (26), genomic *p16* promoter DNA regions encompassing the Sp1-binding elements were immunoprecipitated by the anti-Sp1 antibody. Interestingly, similarly to with the DR1 element, the region encompassing the Sp1A and C sites also bound PPARα in a PPARα ligand–dependent manner (Figure 2D). In contrast, no PPARα binding was observed on the Sp1B site. As negative controls, PCR amplification using primers covering a region localized just downstream of the –1023DR1 site or a β-actin genomic fragment did not yield a significant signal, thus demonstrating the specificity of PPARα immunoprecipitation and PCR amplification. Taken

A
Whole hSMC protein extracts

B
Whole hSMC protein extracts

C
CDK4-immunoprecipitated hSMC proteins


```
Ad-GFP      +    +    –    –
Ad-PPARα    –    –    +    +
GW7647      –    +    –    +
```

D
Whole mSMC protein extracts


```
Wy14,643    –      +      –      +
PPARα      +/+    +/+    –/–    –/–
```
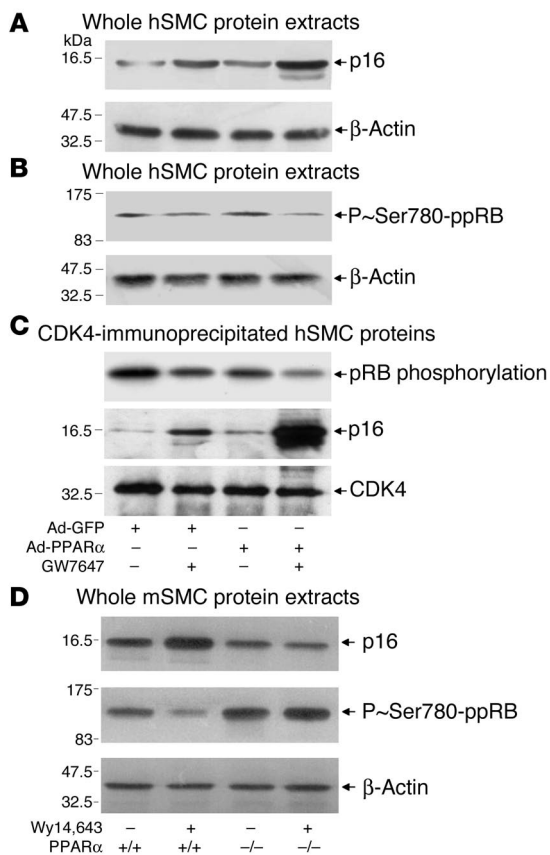
Figure 3
PPARα activation increases p16 protein levels and p16-CDK4 interaction and decreases CDK4-mediated pRB phosphorylation in hSMCs and mSMCs. (**A**–**C**) Protein extracts of hSMCs infected and treated for 12 hours (**A**) or 24 hours (**B** and **C**) with GW7647 (600 nM) were submitted to Western blot analysis either directly (**A** and **B**) or after IP with an anti-CDK4 antibody (**C**). Cellular p16 protein levels (**A**) and in-cell CDK4-mediated pRB phosphorylation (**B**) were measured using an antibody specific for p16 or an anti-pRB antibody recognizing a site specifically phosphorylated by cyclin D1/CDK4 (P~Ser780-ppRB) (28), respectively. (**C**) Anti-CDK4 immunoprecipitates were assayed for kinase activity using the 769–921 pRB fragment as substrate (63) (top panel), or analyzed by Western blot using specific anti-p16 (middle panel) or anti-CDK4 antibodies (lower panel). (**D**) Protein extracts of PPARα$^{-/-}$ or PPARα$^{+/+}$ C57BL/6J mSMCs treated for 24 hours with Wy14,643 (6 μM) were submitted to Western blot analysis using the anti-p16 and anti–P~Ser780-ppRB antibodies.

determined whether the induction of p16 following PPARα activation affected p16/CDK4 interaction and CDK4 activity. To this end, in-cell pRB phosphorylation by CDK4, determined using an anti–P~Ser780-ppRB antibody (28), and in vitro CDK4-associated activity using pRB as substrate were measured after PPARα overexpression and/or activation with GW7647 in hSMCs (Figure 3, B and C, upper panel). In fact, concurring with the decrease of the phosphorylated/nonphosphorylated pRB ratio following PPARα activation (Figure 1C), both analyses indicated that treatment with the PPARα ligand decreases pRB phosphorylation by CDK4 and that this effect is enhanced by PPARα overexpression. Moreover, the levels of p16 associated with CDK4 were increased in hSMCs infected with Ad-PPARα or treated with GW7647, and this interaction was further enhanced in Ad-PPARα–infected GW7647-treated hSMCs (Figure 3C, middle panel). Besides, in-cell p16 protein levels and CDK4-dependent pRB phosphorylation respectively increased and decreased in PPARα$^{+/+}$ but not in PPARα$^{-/-}$ mSMCs following Wy14,643 treatment (Figure 3D).

Finally, the role of p16 in mediating the growth-inhibitory effects of PPARα activation was analyzed in vitro using SMCs isolated from p16$^{-/-}$ mice (29). Strikingly, primary mSMCs isolated

together, these results indicate that PPARα activates the *p16* promoter through direct DNA binding to the p16DR1 site as well as tethering with Sp1 to the proximal Sp1A–C response element.

Induction of p16 following PPARα activation, resulting in the inhibition of CDK4-mediated pRB phosphorylation, is required for the SMC growth-inhibitory activity of PPARα. Next, it was determined whether the upregulation of *p16* gene expression by PPARα results in an increase of p16 protein abundance and in-cell activity. Western blot analysis of hSMC whole-cell protein extracts revealed that PPARα overexpression or GW7647 treatment enhanced p16 protein levels in hSMCs, and the greatest increase was observed when cells were both infected with Ad-PPARα and treated with GW7647 (Figure 3A).

Initially, p16 was identified by virtue of its ability to inhibit G$_1$/S cell-cycle progression by binding to CDK4, thus preventing CDK4 association with D-type cyclins and further initiation of pRB phosphorylation by the cyclin D/CDK4 complexes (8, 9, 27). To verify that PPARα controls p16 function, it was further

Figure 4
p16 deficiency in mSMCs prevents the growth-inhibitory effects of fenofibrate. G$_1$-arrested p16$^{-/-}$ or p16$^{+/+}$ C57BL/6J mSMCs resumed growth at T0 in normal GM containing or not containing Wy14,643 (10 μM). (**A**) Cells were harvested at the indicated times for measurement of DNA content (expressed as arbitrary units). Values are the mean ± SEM of triplicate points from a single experiment (*n* = 3/time point), which was repeated with 3 different cell preparations of primary mSMCs with similar results. (**B**) Cells were arrested after 24 hours for protein extraction followed by Western blot analysis using the anti–P~Ser780-ppRB antibody.

A
mSMCs

B
Whole mSMCs protein extracts


```
Wy14,643    –      –      +
p16        +/+    –/–    –/–
```
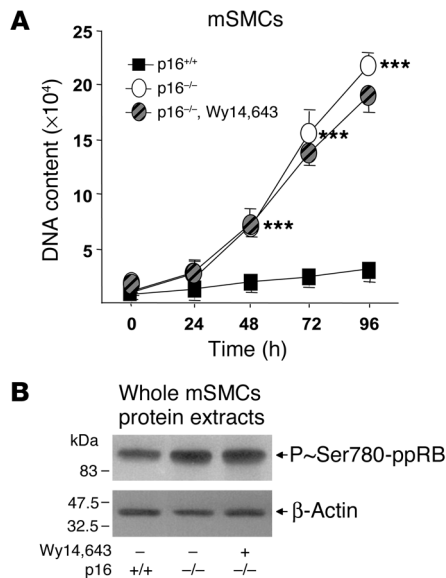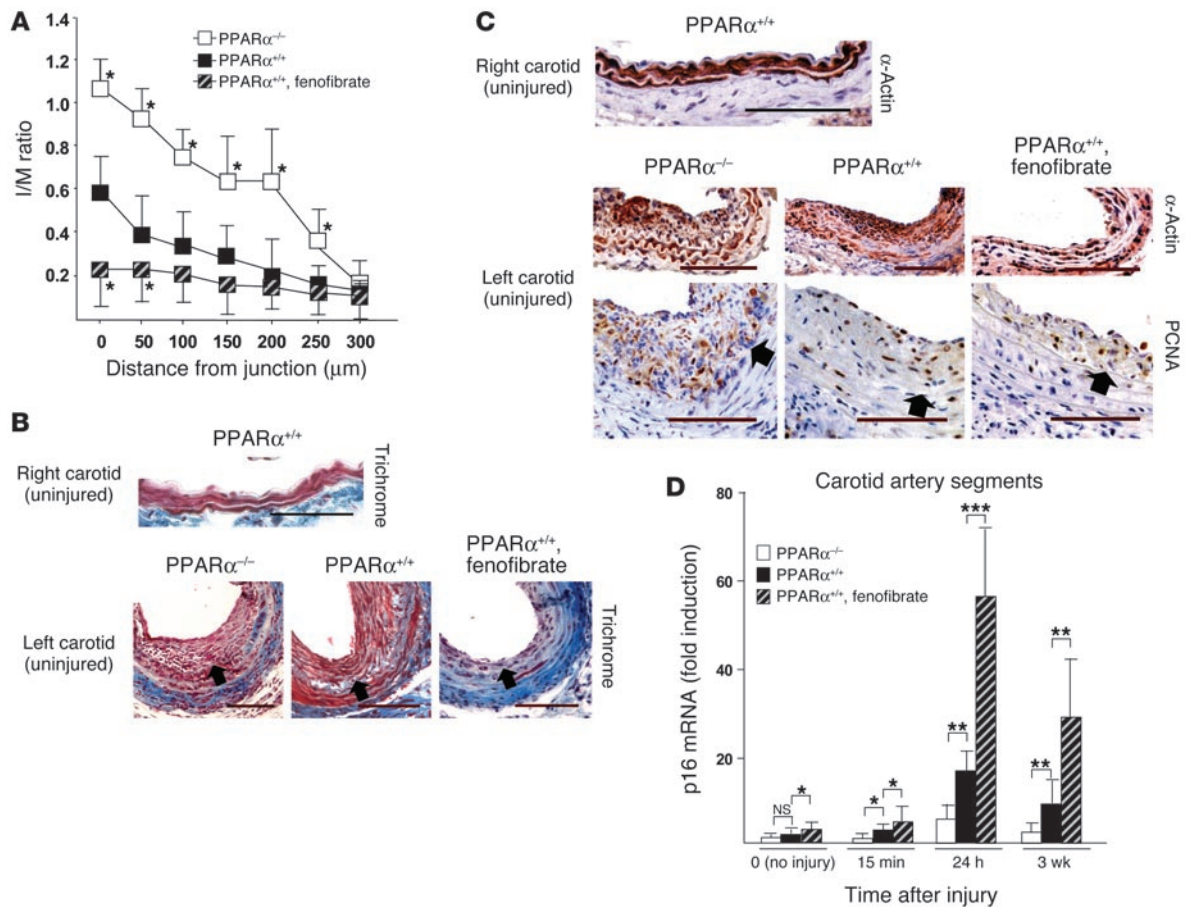
Figure 5
PPARα activation inhibits neointima formation after mechanical carotid injury. Left carotid arteries were performed on PPARα−/− (*n* = 6) or PPARα+/+ Sv/129 mice treated (*n* = 5) or not (*n* = 8) with fenofibrate. (**A**) Topographic pattern of I/M area ratio 3 weeks after injury. Values are mean ± SEM of the I/M ratios measured on Masson's trichrome–stained sections at the indicated distances from the junction between the external and internal branches of the left carotid artery (reference section at 0 μM). *$P \leq 0.05$ vs. wild-type sections. (**B**) Representative carotid sections of uninjured right and injured left carotids at 50 μm from the junction stained with Masson's trichrome. Scale bars: 100 μM. The internal elastic lamina delineating the neointima is indicated by a black arrow. (**C**) Representative sections of mouse carotid arteries immunostained for SMC (α-actin staining, brown, upper panel) or for proliferation marking (PCNA immunostaining to identify cells in S phase, brown, lower panel) at 150 μm and 100 μm from the junction, respectively. No intima was found in uninjured right carotids. Scale bars: 100 μM. The I/M ratio is equal to 0 in uninjured right carotid because intima of the healthy carotid artery is only composed of the monolayer endothelial cells. (**D**) Fenofibrate induces p16 mRNA levels in injured carotid arteries. Mouse carotid arteries were dissected at the indicated times after intraluminal mechanical injury of the left artery. p16 mRNA levels in the carotid segments are expressed as means ± SEM (*n* = 5) of fold change relative to the uninjured wild-type arteries, arbitrarily set to 1. *$P \leq 0.05$, **$P \leq 0.01$, ***$P \leq 0.001$ vs. uninjured wild-type mice.

from p16−/− mice proliferated at a much higher rate than p16+/+ mSMCs (Figure 4A). Moreover, p16−/− mSMCs did not respond to Wy14,643 treatment. Accordingly, the ratio of cell percentage in S compared with G1 phases (data not shown) as well as in-cell CDK4-mediated pRB phosphorylation (Figure 4B) were enhanced in p16−/− mSMCs and not affected by Wy14,643 treatment. Altogether, these data indicate that the G1 cell-cycle arrest induced by ligand-activated PPARα occurs via inhibition of the activity of G1 CDKs, such as CDK4, due to an increased recruitment of p16.

PPARα activation inhibits in vivo SMC proliferation upon carotid arterial injury by increasing p16 gene expression. The in vivo role of PPARα in the control of SMC proliferation was next examined by using a mechanical carotid artery injury mouse model (30) in Sv/129 mice, a strain highly susceptible to intimal hyperplasia (31). The neointimal thickness in response to injury was determined by measuring

the intima/media (I/M) area ratio throughout the entire injured segment starting from the junction between the internal and external left carotid branches. In agreement with previous reports (31, 32), injury induced a marked increase in intimal hyperplasia in wild-type mice as observed 3 weeks after injury (Figure 5, A and B). Interestingly, the I/M ratio was markedly enhanced in PPARα−/− mice, whereas it was drastically decreased in PPARα+/+ mice treated with fenofibrate, whose action in mice requires PPARα expression (33, 34) (Figure 5, A and B). As previously reported (2, 21, 30), SMCs, identified by α-actin staining, were abundantly present in the media of uninjured carotids and constituted the major cell type underlying neointimal development in response to injury in this model (Figure 5, A–C, see PPARα+/+). Moreover, in agreement with the I/M ratio results, neointimal SMC and proliferating cell nuclear antigen–staining (PCNA-staining) were increased in carot-

id sections of PPARα⁻/⁻ mice, and diminished in fenofibrate-treated mice compared with untreated wild-type mice (Figure 5, B and C). In agreement with the in vitro proliferation assays performed in mSMCs (Supplemental Figure 1), PPARα deficiency also provoked hyperplasia in C57BL/6J mice (Supplemental Figure 2), a strain reported to be more resistant to hyperplasia formation after carotid injury (31, 32).

Furthermore, *p16* gene expression was measured in the uninjured carotid segment, which contains mainly SMCs in a quiescent state (1, 4) (Figure 5C), as well as in carotid segments at different times after injury (Figure 5D). Strikingly, p16 mRNA levels were induced after response to injury in PPARα⁺/⁺ but not in PPARα⁻/⁻ mice, an effect that was further enhanced following fenofibrate treatment. A maximal PPARα-dependent induction of p16 mRNA levels was reached within 24 hours and remained elevated 3 weeks after injury. Thus, these data indicate that PPARα activation negatively controls neointima formation in response to injury, possibly via the induction of *p16* gene expression in injured vessels.

Finally, the in vivo role of p16 in mediating the growth-inhibitory effects of PPARα activation were further analyzed using p16⁻/⁻ mice (29). It is noteworthy that, similarly to what occurred in PPARα⁻/⁻ mice (Figure 5 and Supplemental Figure 2), intimal hyperplasia was drastically increased in p16⁻/⁻ mice (Figure 6). An extended neointima formation was observed over the entire lesion segment, which was accompanied by an increase in SMC abundance. Strikingly, fenofibrate treatment did not influence the I/M ratio in these p16⁻/⁻ mice (Figure 6A). Therefore, p16 is required for the inhibitory effects of PPARα activation on vascular SMC growth underlying intimal hyperplasia development.

Discussion

The cardiovascular protective effects of fibrates were initially mainly attributed to a systemic action of PPARα on atherogenic dyslipidemia, characterized by a lowering of triglyceride levels and an increased concentration of plasma HDL-cholesterol concentrations (13). However, a number of recent clinical studies, including the Bezafibrate Coronary Atherosclerosis Intervention Trial (BECAIT; ref. 19), the Lopid Coronary Angiography Trial (LOCAT; ref. 17), and the Diabetes Atherosclerosis Intervention Study (DAIS; ref. 17), have revealed that fibrates inhibit atheromatous plaque progression via effects possibly independent or in addition to their systemic action. These observations are in line with results from in vivo studies performed in rabbits, which indicated that fibrate treatment can inhibit atherosclerosis without affecting plasma lipid profiles (35, 36). Moreover, in the secondary preven-

tion Veterans Administration–HDL-Cholesterol Intervention Trial (VA-HIT), a decreased incidence of cardiovascular events following fibrate treatment was observed, which could not be attributed only to the effects of drug treatment on HDL levels (37). Concurring with these clinical data, compelling mechanistic evidence has recently emerged that PPARα controls cholesterol efflux and the inflammatory response in vessel wall cells (13), highlighting a direct regulatory role of PPARα on vessel wall function. However, despite the crucial role of SMC proliferation in the development of occlusive vascular diseases, the function of PPARα in the control of vascular SMC cell-cycle progression was not yet established. In the present study, we show that PPARα activation inhibits G₁/S cell-cycle progression of both human and mouse primary SMCs in vitro, an effect attributed to the induction of the tumor suppressor gene *p16*. Upregulation of p16 by PPARα agonists results in the sequestration of CDK4 and the consequent decrease of CDK4-mediated pRB phosphorylation, thus providing a mechanism for the SMC G₁ cell-cycle arrest induced by fibrates. The in vivo role of PPARα in the control of SMC proliferation through the induction of *p16* gene expression was further demonstrated by studying the response to mechanical carotid artery injury (30). This carotid injury model is characterized by neointima formation due to an excessive accumulation of SMCs and deposition of extracellular matrix in the intimal layer of the vessel wall, a response which has been proposed to appropriately reflect the "in-stent" restenosis observed in humans (30).

In the search for the molecular mechanisms involved in the p16-dependent growth-inhibitory effects of PPARα on SMCs, PPARα activation was found to upregulate *p16* promoter activity, thus identifying for the first time a molecular mechanism via which PPARα directly interferes with cell-cycle progression. It is noteworthy that numerous common disease predisposition factors and pathways between cancer and vascular remodeling pathologies have been identified, pointing to similarities between the development of both diseases (38). It has been suggested that both vascular diseases and cancer similarly develop from a clonal proliferation of altered cells at the sites of local tissue injury, inflammation, and/or genomic alterations (38). Similar to tumor

Figure 6
p16 deficiency results in the induction of carotid artery hyperplasia that is not inhibited by fenofibrate. Left carotid arteries from p16⁻/⁻ C57BL/6J mice treated or not treated (*n* = 5/group) with fenofibrate were mechanically injured and analyzed after injury as described in Figure 5. (**A**) Topographic pattern of I/M area ratio. Values are mean ± SEM of the I/M ratios measured at the indicated distances from the junction on Masson's trichrome–stained sections. *P ≤ 0.05, **P ≤ 0.01 vs. p16⁺/⁺ mice. No significant difference was found between fenofibrate-treated and untreated p16⁻/⁻ mice. (**B**) Representative sections of mouse carotid arteries stained for morphometry or SMC. Carotid artery sections from untreated mice were stained with Masson's trichrome or with an α-actin antibody at 50 and 25 μM from the junction, respectively. Scale bars: 300 μM. The internal elastic lamina is indicated by black arrows.
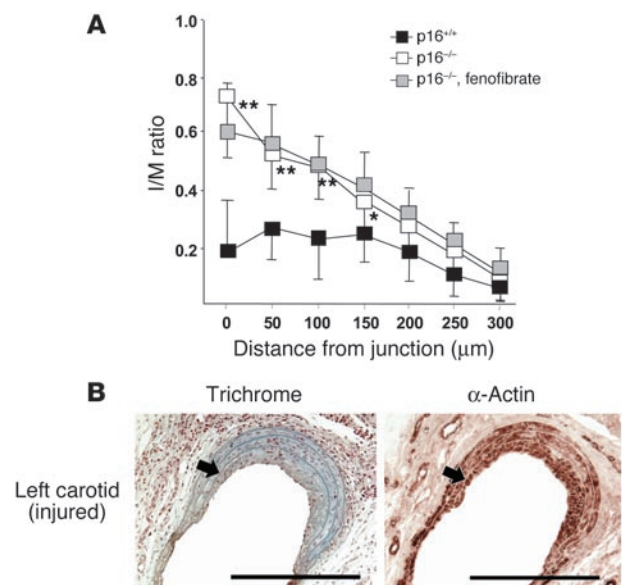
development, the induction of intimal hyperplasia in response to injury involves the conversion of SMCs from a medial non-proliferating differentiated phenotype into a proliferating phenotype associated with pRB hyperphosphorylation (1). However, the molecular mechanisms underlying the relationship between these diseases remain to be characterized. Interestingly, the CDKI and tumor suppressor p27^{Kip1} (p27), whose protein degradation is prevented by PPARγ activators (39), has been shown to inhibit the development of vascular diseases when transferred using an adenoviral vector into balloon-injured porcine arteries (40) as well as through bone marrow–derived immune cells (41). In this study we now report an endogenous regulatory role for the CDKI p16 as SMC growth inhibitor, which furthermore directly mediates the response to fibrates. In fact, p16 expression is correlated to both pRB phosphorylation and expression levels and is required for the negative feedback of G$_1$/S transition (11, 27). Several studies have established that loss of p16 function can be an early event in tumor progression (42, 43) and that it is associated with tumor development (29, 44, 45). Thus, *p16* promoter activity is currently utilized as a prognosis factor for several cancers, such as acute lymphoblastic leukemia, lymphoma, lung carcinoma, and melanoma (45). Here, we identify, for what we believe is the first time, a role for this CDKI, so far studied in cancer pathology, in vascular SMC proliferation underlying occlusive cardiovascular diseases such as restenosis (1).

Strikingly, PPARα deficiency and p16 deficiency both acted as molecular switches inducing SMC proliferation in vitro and in vivo (Figures 1 and 4–6 and Supplemental Figures 1 and 2). Interestingly, the induction of p16 expression alone and in response to fenofibrate treatment was much higher in response to injury than in healthy carotid arteries. Moreover, no significant morphological differences were observed in healthy carotid arteries isolated from untreated PPARα$^{+/+}$ compared with PPARα$^{-/-}$ or fenofibrate-treated mice. Among the genes of the INK4 family, the CDKI p16 is specifically induced in response to oncogenic stress when it acts as a negative retrocontrol of increased pRB phosphorylation (27). In parallel, an important role for PPARα in the response to stress has been demonstrated previously upon fasting (46) or long-term high-fat feeding (47) as well as in the response to inflammatory factors such as leukotriene B4 (48), lipopolysaccharide (LPS), or IL-1 (49). Thus, our results demonstrating that both PPARα and p16 proteins are activated and function locally at the vascular artery injury site further extend these observations of a functional role for PPARα and p16 primarily in the response to stress.

Recently, substantial progress has been made in the prevention of restenosis, notably with the development of stents coated with antimitotic drugs, such as rapamycin (50). However, a potential risk of late thrombus formation associated with incomplete reendothelialization after surgery with these coated stents exists (50). It is noteworthy that, in our mouse model of restenosis, reendothelialization was completed 3 weeks after injury for all studied groups (Supplemental Figure 3). Moreover, thiazolidinedione PPARγ activators —which have previously been shown to control vascular SMC proliferation (39, 51) — were recently shown to reduce coronary in-stent restenosis in type 2 diabetic patients (52, 53). The present report indicates a role for the PPARα/p16 pathway in vascular SMC proliferation in vitro and in a mouse model of restenosis. Further clinical studies are thus warranted to assess whether pharmacological activation of PPARα could provide a novel therapeutic strategy to prevent restenosis in treatments using either systemic administration or coated stents.

Methods

Reagents. Wy14,643 and fenofibric acid were purchased from Sigma-Aldrich and Laboratoires Fournier SA, respectively. GW7647 (25) was kindly provided by P. J. Brown from GlaxoSmithKline (Research Triangle Park, North Carolina, USA).

Reverse transcription and quantitative PCR. RNA extraction, reverse transcription, and quantification of mRNA levels were performed using an MX 4000 apparatus (Stratagene) as previously described (54). 28S RNA was measured as internal control. For in vitro assays, values are expressed as means ± SD of a representative experiment performed in triplicate (for a total of 3 samples measured).

Plasmids and Ad generation. The Sp1 expression plasmid cloned in pcDNA3 was a gift from D. Monté (Institut de Biologie de Lille, Lille, France); the *p16* reporter pGL2 (Promega) constructs were provided by G. Peters (Imperial Cancer Research Fund Laboratories, London, United Kingdom) (11). Mutations of the –1023 p16DR1 were introduced using the QuikChange site-directed mutagenesis kit (Stratagene) and the oligonucleotide mutated p16DR1 (p16DR1mt) (Table 2). The nucleotide positions are indicated relative to the ATG site. Recombinant Ad-GFP and Ad-PPAR were obtained by homologous recombination in *Escherichia coli* (55) after insertion of the cDNAs into the pAdCMV2 vector (Qbiogene). Viral stocks were created and titrated as previously described (56). SMCs (0.5 × 10^6) were infected at an input multiplicity of 100 virus particles/cell by adding virus stocks directly to the culture medium. Efficiency of hSMC infection was between 75–85%, as assessed by FACS analysis with the Ad-GFP vector.

Cell culture assays. Human cervical HeLa cells and primary human aortic SMCs (hSMCs) were obtained from ATCC and BioWhittaker Europe, respectively. HeLa cells were cultured in DMEM medium (Invitrogen Corp.) supplemented with 10% FCS (HyClone), and L-glutamine (2 mM) as well as the antibiotics penicillin (50 U/ml) and streptomycin (55 μg/ml) (Gibco; Invitrogen Corp.). hSMCs were cultured using the SMC Growth Medium 2 Bullet Kit , purchased from BioWhittaker Inc. Mouse primary aortic SMCs (mSMCs) were prepared from aortas of 8- to 12-week-old PPARα$^{+/+}$ or PPARα$^{-/-}$ mice on Sv/129 or C57BL/6J genetic backgrounds or of p16$^{+/+}$ or p16$^{-/-}$ mice on a C57BL/6J genetic background as described (57) and were studied between the third and twelfth passages. mSMCs were cultured in DMEM supplemented with 10% FCS and antibiotics. In all assays, cell synchronization in the G$_0$/G$_1$ phase was induced by serum starvation for at least 24 hours in medium containing 0.4% FCS. To reinduce cell proliferation, cells were reincubated in routine GM (time 0 or T0 of the experiments). At T0, mSMCs were treated with the indicated PPARα ligand or an identical volume of Me$_2$SO (vehicle). hSMCs were infected overnight and subsequently treated with PPARα ligands or vehicle as indicated. Three independent preparations from different mice were studied for each primary SMC type and resulted in similar results.

For cell proliferation assays, cellular DNA content was determined using fluorochrome 3,5-diaminobenzoicacid free acid (DABA) as described previously (58). Flow cytometry analysis profiles were determined by propidium iodide staining of nuclear DNA as described (59).

For transient transfection assays, HeLa cells in 24-well plates at an initial density of 1.5 × 10^4 per well were transfected with ExGen 500 (Euromedex) at a ratio of 4 μl ExGen 500/0.5 μg of DNA. The indicated pGL2 reporter constructs (100 ng) were cotransfected with the indicated expression vectors and the internal control *Renilla* luciferase reporter plasmid pRL-null (10 ng). The amount of plasmids in the transfection mixture was equalized to 0.5 μg by adding pcDNA3 vector. After 12 hours, cells were incubated

for an additional 10 hours in fresh medium supplemented with fenofibric acid (100 μM) or Me₂SO (vehicle). Luciferase activity was assessed with the Dual-Luciferase Reporter Assay System (Promega) as previously described (54). Transfections were carried out in triplicate, and each experiment was repeated at least 3 times.

Protein assays. Cells were washed twice with ice-cold PBS and then collected in ice-cold RIPA buffer (1× PBS, 1% Nonidet P-40, 0.5% sodium deoxycholate, 0.1% SDS, phosphatase and protease inhibitors) or kinase lysis buffer (50 mM Tris, pH 8.0, 0,1% IGEPAL; Sigma-Aldrich). Lysates were incubated for 30 minutes on ice, and cell debris was removed by centrifugation. Extracts were then aliquoted and stored at –80°C.

For coimmunoprecipitation assays, whole-cell lysates were preincubated with 1.0 μg nonimmune rabbit IgG and 20 μl of protein A-Sepharose beads (Amersham Biosciences) during 30 minutes at 4°C and centrifuged. Cleared lysates (1 mg) were immunoprecipitated for 1 hour at 4°C with the anti-CDK4 antibody (RB-016, Microm Microtech France) and then incubated overnight at 4°C with protein A-Sepharose. The immunoprecipitated proteins were washed with lysis buffer and resuspended in electrophoresis sample buffer.

Samples of immunoprecipitated or total proteins (20–30 μg) were analyzed by Western blot using the following primary antibodies: anti-CDK4 (RB-003; Microm Microtech France), anti-p16 (554079 for hSMCs, BD Biosciences — Pharmingen; and MS-887 for mSMCs, Microm Microtech France), anti-pRB (554136; BD Biosciences — Pharmingen), anti–P~Ser780–phosphorylated pRB (anti–P~Ser780-ppRB) (sc-12901; Santa Cruz Biotechnology Inc.) raised against a pRB peptide phosphorylated on Ser-780, and anti–β-actin (sc-7210; Santa Cruz Biotechnology Inc.) for loading control. Each blot is representative of 3 independent experiments. We have verified that immunoprecipitation with nonspecific IgG followed by Western blot analyses using anti-p16 or anti-CDK4 antibodies did not yield any signal (data not shown).

In vitro CDK4 activity was measured as previously described by Draetta et al. (60) using CDK4-immunoprecipitated SMC extracts (1 mg), a peptide corresponding to the carboxy terminal domain of pRB (sc-4112; Santa Cruz Biotechnology Inc.) as substrate, as well as 1 mg/ml casein (Sigma-Aldrich) in the assay buffer. After 5 minutes of preincubation at 30°C, the reaction was initiated by the addition of 1 μM adenosine triphosphate (ATP) and 5 μCi [γ-³²P]ATP and continued at 30°C for 1 hour. Fifteen microliters of electrophoresis buffer (3×) was added to stop the reaction, and the samples were resolved on a 10% SDS-PAGE gel.

EMSAs. Human PPARα and mouse RXRα proteins were synthesized in vitro, and EMSAs were performed with double-stranded oligonucleotides (Table 2) end-labeled with [γ-³²P]ATP as previously described (54). Competition experiments were performed by adding a 300-M excess of the indicated unlabeled oligonucleotides to the binding reaction just before the addition of the labeled probes. For supershift experiments, 0.2 μg anti-PPARα antibody (sc-9000; Santa Cruz Biotechnology Inc.) was preincubated for 20 minutes on ice in the binding buffer before addition of DNA probes.

ChIP assays. ChIP experiments were performed as previously described (54). At 2 hours and 30 minutes before harvesting, hSMCs were washed with serum-free DMEM medium containing 0.2% bovine serum albumin and incubated in this medium with either fenofibric acid (250 μM) or Me₂SO (vehicle) as control. Cells were sonicated and lysates immunoprecipitated using the indicated antibodies. Extracted DNA was PCR amplified using specific primers for the *p16* and the *β-actin* gene promoters (see Table 2) (54). An equal volume of nonprecipitated (input) genomic DNA was amplified as positive control. One-fifteenth (input) or one-fifth (precipitated DNA) of PCR products were separated on an ethidium-bromide-stained 2% agarose gel.

Animals. All animal experiments were conducted with the approval of the Pasteur Institute review board, Lille, France, following guidelines for animal care and use (61). Studies were performed on 8- to 10-week-old PPARα⁺/⁺ and PPARα⁻/⁻ mice with Sv/129 or C57BL/6J genetic backgrounds (a kind gift of F. Gonzalez, National Cancer Institute, NIH, Bethesda, Maryland, USA; ref. 62) as well as p16⁻/⁻ mice with a C57BL/6J genetic background (30). One group of p16⁺/⁺ or p16⁻/⁻ mice was treated orally with fenofibrate at 0.05% in chow diet (i.e., 50 mg/kg body weight/day) for 1 week before and 3 weeks after the surgical procedure. For the surgical procedures, the mice were anesthetized by intraperitoneal injection with a solution of domitor (0.68 mg/kg) and ketamin (67 mg/kg) (Orion Pharma) and allowed to recover on cotton following subcutaneous injection of the antidote antisedan at 1.7 mg/kg (Orion Pharma). At 3 weeks after injury, mice were anesthetized and then sacrificed by overdose of domitor/ketamin.

Carotid arterial injury model. Intraluminal mechanical injury of the carotid arteries was performed by rupture of the internal elastic lamina and endothelial layer removal according to the method described by Carmeliet et al. (30). Briefly, the left internal carotid artery was exposed by blunt-end dissection, tied off distally, and looped proximally on the external branch with 5.0 silk black suture (Harvard apparatus unit; Ealing SA). A transverse section was made in the proximal portion of the external carotid artery, and a straight wire guide (C-SF-15-15; Cook) was passed toward the aortic arch and withdrawn 3 times with a rotating motion. After removal of the wire, the distal portion of the external carotid artery was tied off, and the skin incision was closed.

Tissue harvest, histology, and immunohistochemistry. Tissue harvesting, fixation, embedding, and sectioning were performed as described by Carmeliet et al. (30), with slight modifications. The mice serving for morphometric analyses were first perfusion fixed with 4% phosphate-buffered formalin (pH 7.0) or methanol at physiological pressure. The left injured and corresponding right vessel segments were dissected and post-fixed overnight in 4% formalin or methanol placed between Whatman filter paper and then transferred to cold PBS. The vessel segments were then dehydrated in graded ethanol baths, cleared in toluene, and embedded in paraffin. Sections (6 μm) were created throughout the whole approximate 350-μm dissected fragment from the junction. Distance from junction was measured as the length between the junction of the external and internal branches of the left carotid artery (reference section at 0 μM, which appears right after the beginning of the injury) and the section position.

Sections at 50-μm increments starting from the junction were stained with Masson's trichrome reagent (Sigma-Aldrich) according to the manufacturer's protocol. The sections were immunohistochemically stained with a mouse monoclonal anti–α-actin antibody (1:100 dilution; Sigma-Aldrich) for SMC labeling, followed by detection with biotinylated secondary antibodies and streptavidin-horseradish peroxidase. Detection of PCNA was performed using a ready-to-use HRP-conjugated anti-PCNA monoclonal mouse antibody (DakoCytomation). Immunostains were visualized using the DAB substrate–chromogen system (DakoCytomation) for α-actin and PCNA. Nuclear counterstaining was performed with hematoxylin. Images were captured by use of a JVC 3-CCD video camera.

Morphometric analyses. Masson's-stained sections were analyzed blindly by 2 observers using the computer-assisted Quips Image analysis system (Leica Mikroskopie und Systeme GmbH). Quantitative measurements of the neointima (i.e., luminal part limited by the internal elastic lamina) and media (i.e., part delineated by external and internal elastic laminas) area were made on complete cross-sectioned carotid arteries stained with Masson's trichrome. Neointimal thickness was expressed as the ratio of the area of the neointima to the area of the media.

Statistics. For in vitro assays, statistical differences were analyzed by the unpaired Student's *t* test. For morphometric analyses, statistical differences

in I/M ratio of PPARα^{−/−} or fenofibrate-treated versus untreated PPARα^{+/+} mice were determined by ANOVA followed by Wilcoxon's signed-rank analysis. Statistical significance was set at a value of $P \leq 0.05$.

1. Dzau, V.J., Braun-Dullaeus, R.C., and Sedding, D.G. 2002. Vascular proliferation and atherosclerosis: new perspectives and therapeutic strategies. *Nat. Med.* **8**:1249–1256.
2. Hao, H., Gabbiani, G., and Bochaton-Piallat, M.L. 2003. Arterial smooth muscle cell heterogeneity: implications for atherosclerosis and restenosis development. *Arterioscler. Thromb. Vasc. Biol.* **23**:1510–1520.
3. Ross, R. 1999. Atherosclerosis–an inflammatory disease. *N. Engl. J. Med.* **340**:115–126.
4. Yoshida, T., and Owens, G.K. 2005. Molecular determinants of vascular smooth muscle cell diversity. *Circ. Res.* **96**:280–291.
5. Walworth, N.C. 2000. Cell-cycle checkpoint kinases: checking in on the cell cycle. *Curr. Opin. Cell Biol.* **12**:697–704.
6. Harbour, J.W., and Dean, D.C. 2000. Rb function in cell-cycle regulation and apoptosis. *Nat. Cell Biol.* **2**:E65–E67.
7. Ekholm, S.V., and Reed, S.I. 2000. Regulation of G(1) cyclin-dependent kinases in the mammalian cell cycle. *Curr. Opin. Cell Biol.* **12**:676–684.
8. Serrano, M., Hannon, G.J., and Beach, D. 1993. A new regulatory motif in cell-cycle control causing specific inhibition of cyclin D/CDK4. *Nature.* **366**:704–707.
9. Tam, S.W., Shay, J.W., and Pagano, M. 1994. Differential expression and cell cycle regulation of the cyclin-dependent kinase 4 inhibitor p16Ink4. *Cancer Res.* **54**:5816–5820.
10. Parry, D., Bates, S., Mann, D.J., and Peters, G. 1995. Lack of cyclin D-Cdk complexes in Rb-negative cells correlates with high levels of p16INK4/MTS1 tumour suppressor gene product. *EMBO J.* **14**:503–511.
11. Hara, E., et al. 1996. Regulation of p16CDKN2 expression and its implications for cell immortalization and senescence. *Mol. Cell. Biol.* **16**:859–867.
12. Michalik, L., Desvergne, B., and Wahli, W. 2004. Peroxisome-proliferator-activated receptors and cancers: complex stories. *Nat. Rev. Cancer.* **4**:61–70.
13. Marx, N., Duez, H., Fruchart, J.C., and Staels, B. 2004. Peroxisome proliferator-activated receptors and atherogenesis: regulators of gene expression in vascular cells. *Circ. Res.* **94**:1168–1178.
14. Brown, W.V. 1987. Potential use of fenofibrate and other fibric acid derivatives in the clinic. *Am. J. Med.* **83**:85–89.
15. Willson, T.M., Brown, P.J., Sternbach, D.D., and Henke, B.R. 2000. The PPARs: from orphan receptors to drug discovery. *J. Med. Chem.* **43**:527–550.
16. Robins, S.J., et al. 2001. Relation of gemfibrozil treatment and lipid levels with major coronary events: VA-HIT: a randomized controlled trial. *JAMA.* **285**:1585–1591.
17. Steiner, G. 1996. The Diabetes Atherosclerosis Intervention Study (DAIS): a study conducted in cooperation with the World Health Organization. The DAIS Project Group. *Diabetologia.* **39**:1655–1661.
18. Frick, M.H., et al. 1997. Prevention of the angiographic progression of coronary and vein-graft atherosclerosis by gemfibrozil after coronary bypass surgery in men with low levels of HDL cholesterol. Lopid Coronary Angiography Trial (LOCAT) Study Group. *Circulation.* **96**:2137–2143.
19. Ericsson, C.G., et al. 1996. Angiographic assessment of effects of bezafibrate on progression of coronary artery disease in young male postinfarction patients. *Lancet.* **347**:849–853.
20. Staels, B., et al. 1998. Mechanism of action of fibrates on lipid and lipoprotein metabolism. *Circulation.* **98**:2088–2093.
21. Zahradka, P., et al. 2003. Activation of peroxisome proliferator-activated receptors alpha and gamma1 inhibits human smooth muscle cell proliferation. *Mol. Cell. Biochem.* **246**:105–110.
22. Staels, B., et al. 1998. Activation of human aortic smooth-muscle cells is inhibited by PPAR-alpha but not by PPARgamma activators. *Nature.* **393**:790–793.
23. Marx, N., Schonbeck, U., Lazar, M.A., Libby, P., and Plutzky, J. 1998. Peroxisome proliferator-activated receptor gamma activators inhibit gene expression and migration in human vascular smooth muscle cells. *Circ. Res.* **83**:1097–1103.
24. Nigro, J., Dilley, R.J., and Little, P.J. 2002. Differential effects of gemfibrozil on migration, proliferation and proteoglycan production in human vascular smooth muscle cells. *Atherosclerosis.* **162**:119–129.
25. Brown, P.J., et al. 2001. Identification of a subtype selective human PPARalpha agonist through parallel-array synthesis. *Bioorg. Med. Chem. Lett.* **11**:1225–1227.
26. Myohanen, S., and Baylin, S.B. 2001. Sequence-specific DNA binding activity of RNA helicase A to the p16INK4a promoter. *J. Biol. Chem.* **276**:1634–1642.
27. Sherr, C.J., and Roberts, J.M. 1999. CDK inhibitors: positive and negative regulators of G1-phase progression. *Genes Dev.* **13**:1501–1512.
28. Kitagawa, M., et al. 1996. The consensus motif for phosphorylation by cyclin D1-Cdk4 is different from that for phosphorylation by cyclin A/E-Cdk2. *EMBO J.* **15**:7060–7069.
29. Krimpenfort, P., Quon, K.C., Mooi, W.J., Loonstra, A., and Berns, A. 2001. Loss of p16Ink4a confers susceptibility to metastatic melanoma in mice. *Nature.* **413**:83–86.
30. Carmeliet, P., et al. 1997. Urokinase but not tissue plasminogen activator mediates arterial neointima formation in mice. *Circ. Res.* **81**:829–839.
31. Wang, X., and Paigen, B. 2002. Comparative genetics of atherosclerosis and restenosis: exploration with mouse models. *Arterioscler. Thromb. Vasc. Biol.* **22**:884–886.
32. Kuhel, D.G., Zhu, B., Witte, D.P., and Hui, D.Y. 2002. Distinction in genetic determinants for injury-induced neointimal hyperplasia and diet-induced atherosclerosis in inbred mice. *Arterioscler. Thromb. Vasc. Biol.* **22**:955–960.
33. Gonzalez, F.J., Peters, J.M., and Cattley, R.C. 1998. Mechanism of action of the nongenotoxic peroxisome proliferators: role of the peroxisome proliferator-activator receptor alpha. *J. Natl. Cancer Inst.* **90**:1702–1709.
34. Kockx, M., et al. 1999. Fibrates suppress fibrinogen gene expression in rodents via activation of the peroxisome proliferator-activated receptor-alpha. *Blood.* **93**:2991–2998.
35. Saitoh, K., et al. 1995. Anti-atheromatous effects of fenofibrate, a hypolipidemic drug. I: Anti-atheromatous effects are independent of its hypolipidemic effect in cholesterol-fed rabbits [In Japanese]. *Nippon Yakurigaku Zasshi.* **106**:41–50.
36. Saitoh, K., Mori, T., Kasai, H., Nagayama, T., and Ohbayashi, S. 1995. Anti-atheromatous effects of fenofibrate, a hypolipidemic drug. II: Anti-atheromatous effects are independent of its hypolipidemic effect in hereditary hyperlipidemic rabbits [In Japanese]. *Nippon Yakurigaku Zasshi.* **106**:51–60.
37. Rubins, H.B., et al. 1999. Gemfibrozil for the secondary prevention of coronary heart disease in men with low levels of high-density lipoprotein cholesterol. Veterans Affairs High-Density Lipoprotein Cholesterol Intervention Trial Study Group. *N. Engl. J. Med.* **341**:410–418.
38. Ross, J.S., Stagliano, N.E., Donovan, M.J., Breitbart, R.E., and Ginsburg, G.S. 2001. Atherosclerosis and cancer: common molecular pathways of disease development and progression. *Ann. N. Y. Acad. Sci.* **947**:271–292; discussion 292–293.
39. Wakino, S., et al. 2000. Peroxisome proliferator-activated receptor gamma ligands inhibit retinoblastoma phosphorylation and G1--> S transition in vascular smooth muscle cells. *J. Biol. Chem.* **275**:22435–22441.
40. Tanner, F.C., et al. 2000. Differential effects of the cyclin-dependent kinase inhibitors p27(Kip1), p21(Cip1), and p16(Ink4) on vascular smooth muscle cell proliferation. *Circulation.* **101**:2022–2025.
41. Boehm, M., et al. 2004. Bone marrow–derived immune cells regulate vascular disease through a p27(Kip1)-dependent mechanism. *J. Clin. Invest.* **114**:419–426. doi:10.1172/JCI200420176.
42. Belinsky, S.A., et al. 1998. Aberrant methylation of p16(Ink4a) is an early event in lung cancer and a potential biomarker for early diagnosis. *Proc. Natl. Acad. Sci. U. S. A.* **95**:11891–11896.
43. Nuovo, G.J., Plaia, T.W., Belinsky, S.A., Baylin, S.B., and Herman, J.G. 1999. In situ detection of the hypermethylation-induced inactivation of the p16 gene as an early event in oncogenesis. *Proc. Natl. Acad. Sci. U. S. A.* **96**:12754–12759.
44. Wong, D.J., Foster, S.A., Galloway, D.A., and Reid, B.J. 1999. Progressive region-specific de novo methylation of the p16 CpG island in primary human mammary epithelial cell strains during escape from M(0) growth arrest. *Mol. Cell. Biol.* **19**:5642–5651.
45. Sharpless, N.E., and DePinho, R.A. 1999. The INK4A/ARF locus and its two gene products. *Curr. Opin. Genet. Dev.* **9**:22–30.
46. Kersten, S., et al. 1999. Peroxisome proliferator-activated receptor alpha mediates the adaptive response to fasting. *J. Clin. Invest.* **103**:1489–1498.
47. Guerre-Millo, M., et al. 2001. PPAR-alpha-null mice are protected from high-fat diet-induced insulin resistance. *Diabetes.* **50**:2809–2814.
48. Devchand, P.R., et al. 1996. The PPARalpha-leukotriene B4 pathway to inflammation control. *Nature.* **384**:39–43.
49. Gervois, P., et al. 2004. Global suppression of IL-6-

induced acute phase response gene expression after chronic in vivo treatment with the peroxisome proliferator-activated receptor-alpha activator fenofibrate. *J. Biol. Chem.* **279**:16154–16160.

50. Froeschl, M., Olsen, S., Ma, X., and O'Brien, E.R. 2004. Current understanding of in-stent restenosis and the potential benefit of drug eluting stents. *Curr. Drug Targets Cardiovasc. Haematol. Disord.* **4**:103–117.

51. Law, R.E., et al. 1996. Troglitazone inhibits vascular smooth muscle cell growth and intimal hyperplasia. *J. Clin. Invest.* **98**:1897–1905.

52. Takagi, T., et al. 2003. Pioglitazone reduces neointimal tissue proliferation after coronary stent implantation in patients with type 2 diabetes mellitus: an intravascular ultrasound scanning study. *Am. Heart J.* **146**:E5.

53. Choi, D., et al. 2004. Preventative effects of rosiglitazone on restenosis after coronary stent implantation in patients with type 2 diabetes. *Diabetes Care.* **27**:2654–2660.

54. Barbier, O., et al. 2003. FXR induces the UGT2B4 enzyme in hepatocytes: a potential mechanism of negative feedback control of FXR activity. *Gastroenterology.* **124**:1926–1940.

55. Chartier, C., et al. 1996. Efficient generation of recombinant adenovirus vectors by homologous recombination in Escherichia coli. *J. Virol.* **70**:4805–4810.

56. Sardet, C., et al. 1995. E2F-4 and E2F-5, two members of the E2F family, are expressed in the early phases of the cell cycle. *Proc. Natl. Acad. Sci. U. S. A.* **92**:2403–2407.

57. Corsini, A., et al. 1996. Effect of the new calcium antagonist lercanidipine and its enantiomers on the migration and proliferation of arterial myocytes. *J. Cardiovasc. Pharmacol.* **28**:687–694.

58. Fiszer-Szafarz, B., Szafarz, D., and Guevara de Murillo, A. 1981. A general, fast, and sensitive micromethod for DNA determination application to rat and mouse liver, rat hepatoma, human leukocytes, chicken fibroblasts, and yeast cells. *Anal. Biochem.* **110**:165–170.

59. Kherrouche, Z., De Launoit, Y., and Monte, D. 2004. Human E2F6 is alternatively spliced to generate multiple protein isoforms. *Biochem. Biophys. Res. Commun.* **317**:749–760.

60. Draetta, G., Brizuela, L., Potashkin, J., and Beach, D. 1987. Identification of p34 and p13, human homologs of the cell cycle regulators of fission yeast encoded by cdc2+ and suc1+. *Cell.* **50**:319–325.

61. Vu-Dac, N., et al. 1997. Transcriptional regulation of apolipoprotein A-I gene expression by the nuclear receptor RORalpha. *J. Biol. Chem.* **272**:22401–22404.

62. Lee, S.S., et al. 1995. Targeted disruption of the alpha isoform of the peroxisome proliferator-activated receptor gene in mice results in abolishment of the pleiotropic effects of peroxisome proliferators. *Mol. Cell. Biol.* **15**:3012–3022.

63. Zarkowska, T., and Mittnacht, S. 1997. Differential phosphorylation of the retinoblastoma protein by G1/S cyclin-dependent kinases. *J. Biol. Chem.* **272**:12738–12746.

64. Gizard, F., et al. 2004. The transcriptional regulating protein of 132 kDa (TReP-132) differentially influences steroidogenic pathways in human adrenal NCI-H295 cells. *J. Mol. Endocrinol.* **32**:557–569.